Electrochimica Acta 166 (2015) 32–39

Contents lists available at ScienceDirect

Electrochimica Acta

journal homepage: www.elsevier.com/locate/electacta

Prussian Green: A High Rate Capacity Cathode for Potassium Ion Batteries

Prasanna Padigi [a,1,*], Joseph Thiebes [b,1], Mitchell Swan [b,1], Gary Goncher [b,1], David Evans [b,1], Raj Solanki [a,b,2]

[a] Electrical and Computer Engineering, Portland State University, Portland, OR 97201, United States
[b] Department of Physics, Portland State University, Portland, OR 97201, United States

ARTICLE INFO

Article history:
Received 23 December 2014
Received in revised form 3 March 2015
Accepted 12 March 2015
Available online 14 March 2015

Keywords:
Potassium ion battery
Prussian Green
Aqueous rechargeable battery
Cathode

ABSTRACT

The influence of the precursors, namely potassium ferrocyanide and potassium ferricyanide on the particles sizes of Prussian Blue (PB) and Prussian Green (PG), under identical reaction conditions have been investigated. It was found that the particle sizes influence the gravimetric capacity utilization of these materials as cathodes for aqueous potassium (K^+) ion batteries. The PG particle sizes were on the order of 50–75 nm, whereas PB particles size were on the order of 2–10 microns. The PG cathodes demonstrated a reversible capacity of 121.4 mAhr/g, with a coulombic efficiency of 98.7% compared to PB cathodes which demonstrated 53.8 mAhr/g, with a coulombic efficiency of 100%. We interpret the increased capacity of PG batteries relative to PB batteries as being a result of the smaller particle size of PG, which results in greater accessibility of the cathode to K+ ions.

1. Introduction

Prussian blue (PB) belongs to a family of transition metal hexacyanometallates that are composed of mixed valence compounds. It is non-toxic as well as inexpensive and easy to synthesize. It has been used as a pigment for about three centuries and more recently to treat patients who have ingested radioactive materials [1], as sensor electrodes [2,3] and as a rechargeable battery cathode [4–9]. Its chemical composition in the "soluble form" is $KFe^{III}Fe^{II}(CN)_6$. Oxidation of this material leads to formation of Prussian Green (PG), sometimes referred to as Berlin Green), represented by the chemical composition $Fe^{III}Fe^{III}(CN)_6$. PB and PG possess a face centered cubic (FCC) lattice with a perovskite-like structure [10] that has a large channel for the diffusion of ions as indicated in Figs. 1(a) and 1(b), respectively. The structure contains a cyanide ligand (CN^-) which acts as a bridge between the Fe^{2+} and Fe^{3+} ions in the case of PB and $Fe^{3+}$and Fe^{3+} ions in the case of PG, leading to a cubic structure with the unit cell parameters $a_0 = b_0 = c_0$ of about 10.2 Å. According to the hard sphere model, the interstitial space is about 1.6 Å [7]. Figs. 1(a) and 1(b) show lattice structures of Prussian Blue and Prussian Green that have been drawn to scale. The CN^- ions in the lattice are depicted with a length of 3.54 Å [13]. The CN bond length in Prussian Blue is 1.13 Å [14]. In theory, both PB and PG possess approximately the same theoretical capacity of 155.52 mAhr/g for K^+ ion intercalation and are expected to have similar electrochemical behavior. PB and PG are very stable materials due to the strong bonding between the carbon end of the cyanide ligand and the partially filled d-orbitals of the Fe^{2+} (PB) and Fe^{3+} (PG) ions as well as the bonding between the nitrogen end of the cyanide ligand and the partially filled d-orbitals of the Fe^{3+} ions.

Li-ion batteries have been the mainstay of high density energy storage devices over the past decade. Lithium salts are expensive, resulting in a higher cost per kilowatt-hour (kWh) of stored power in Li-ion batteries. In order to increase the practicality of grid level energy storage using batteries by decreasing the cost, it is imperative to explore alternatives to lithium salts.

One such alternative is potassium (K^+). Potassium salts are widely available in large quantities and at a lower cost than lithium salts. With a hydrated size of 1.25 Å, K^+ ions are well suited to being used as a guest species for intercalation in PB and PG as electrode materials. Although aqueous K^+ ion intercalation type batteries have a lower voltage than Li+, they offer a low cost alternative for a high capacity, high rate capability and safe option for grid level energy storage. In general, Prussian blue analogues (PBAs) have been shown to have long life at a high rate of charge/discharge for K^+ ions [7]. However, these materials lack high capacity due to a

* Corresponding author. Tel.: +1 971 285 0496; fax: +1 503 725 2815.
E-mail address: spadigi@pdx.edu (P. Padigi).
[1] SRTC, 1719 SW 10th Ave, SB2-55, Portland State University, Portland, OR 97201, USA.
[2] SRTC, 1719 SW 10th Ave, SB2-56, Portland State University, Portland, OR 97201, USA.

http://dx.doi.org/10.1016/j.electacta.2015.03.084
0013-4686/

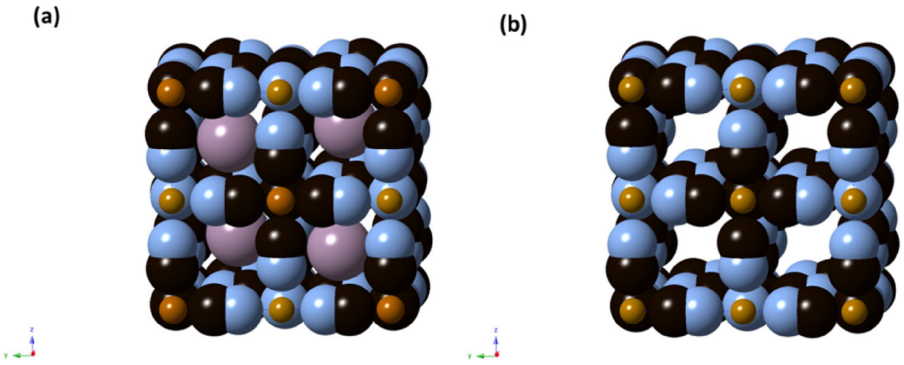

Fig. 1. (a). Crystal lattice unit cell of Prussian Blue (PB) with intercalated K^+. (b). Crystal lattice unit cell of Prussian Green (PG).

single step insertion and extraction of K^+ ions during discharging and charging of the electrodes, respectively, due to inaccessibility of redox activity at the second metal ion. Prussian green (PG), on the other hand allows for a dual step insertion and extraction of K^+ ions, potentially leading to nearly double the capacity demonstrated by PBAs with single step insertion process. In our current investigation, Prussian Green (PG) has been evaluated as a cathode material for aqueous K^+-ion intercalation-type rechargeable battery and its performance is compared against its partially reduced form Prussian Blue (PB).

2. Experimental Section

2.1. Synthesis

Prussian Green: Prussian green ($Fe^{III}Fe^{III}(CN)_6$) was synthesized by a wet chemical precipitation technique. Equimolar concentrations of ferric nitrate ($Fe(NO_3)_3$) and potassium ferricyanide ($K_3Fe(CN)_6$) solutions (5 mmoles in 15 ml deionized water) were mixed together through drop-wise addition of ferric nitrate solution to potassium ferricyanide solution at 60 °C under constant stirring for 2 hours, resulting in the initial formation of a brown precipitate which gradually turned green. The precipitate was repeatedly cleaned (five times) using deionized (DI) water and methanol by centrifugation at about 7,000 rpm for 5 minutes. The precipitate was then dried at room temperature under ambient conditions.

Prussian Blue: Prussian blue ($KFe^{III}Fe^{II}(CN)_6$) was synthesized using the same technique as described above for the synthesis of Prussian green. The main difference was that equimolar concentrations of ferric nitrate ($Fe(NO_3)_3$) and potassium ferrocyanide ($K_4Fe(CN)_6$) solutions (5 mmoles in 15 ml deionized water) were mixed together through drop-wise addition of ferric nitrate solution to potassium ferrocyanide solution at 60 °C under constant stirring for 2 hours, resulting in the formation of a blue precipitate. The precipitate °was cleaned using the same procedure as above.

Prussian Green (PG-HT): PG-HT ($Fe^{III}Fe^{III}(CN)_6$) was also synthesized using a hydrothermal technique, where equimolar concentrations of ferric nitrate ($Fe(NO_3)_3$) and potassium ferricyanide ($K_3Fe(CN)_6$) solutions (5 mmoles in 15 ml deionized water) were mixed together through drop-wise addition of ferric nitrate solution to potassium ferricyanide solution at room temperature, resulting in the immediate formation of a brown precipitate. The solution was then transferred to a 50 ml capacity Teflon lined stainless steel hydrothermal reactor and the solution level was raised to a total volume of 40 ml by adding an additional 10 ml of DI water. The reactor was sealed and subjected to a temperature of 60 °C for 24 hours resulting in a green precipitate. The reactor was allowed to cool slowly to room temperature after which the precipitate was cleaned using water and methanol through centrifugation at about 7,000 rpm for 5 minutes. The precipitate was then dried at room temperature under ambient conditions.

2.2. Characterization

The physical morphology and the phase composition of the Prussian Green, Prussian Blue, and hydrothermally synthesized Prussian Green samples were characterized using scanning electron microscopy, energy dispersive X-ray analysis (EDAX) and powder X-ray diffractometry (PXRD). PXRD data was collected in a focused beam (Bragg–Brentano) geometry on a Rigaku Model Ultima IV X-ray diffraction system using graphite-monochromatized Cu Kα radiation. Scans were performed over an angular range of 10°–70° 2θ at room temperature. Cyclic voltammetry and galvanic cycling was performed with an EG&G 273A potentiostat.

2.3. Electrochemistry

The electrochemical performance of active materials (PG, PB and PG-HT) was evaluated using cyclic voltammetry (CV) and galvanic cycling (GC) at ambient temperature. The test cell was comprised of glass container with three electrodes, where a graphite rod acted as a counter electrode, carbon paper coated with active material was the working electrode, and an Ag/AgCl (saturated KCl) filled capillary tube was a reference electrode. All the measurements were made with 0.5 cm^2 of the working electrode exposed to the electrolyte solution. The stock electrolyte for all measurements was composed of 1 M KNO_3 in DI water. The cathode composite electrode was prepared by mixing the active material powder with multi-walled carbon nanotubes, carbon black, and polyvinylidene fluoride (PVDF) binder in a ratio of 80:9:2:9. The mixture was finely ground using a mortar and pestle. A slurry was prepared by adding a few drops of N-methyl-2-pyrrolidone (NMP) to the above formed homogeneous powder and spread on both sides of a carbon paper which acted as the current collector. The positive electrode material loading was about 3.6 mg/cm^2. The slurry coated electrodes were initially dried at room temperature and further dried under vacuum at 100 °C for 1 hour. In the present work, charging is represented by extraction of K^+ ions from the lattice of the active material and discharging by insertion of K^+ ions into the lattice of the active material. For charge-discharge measurements, the PG electrodes were subjected to three different current densities of 111 mA/g, 277 mA/g, and 388 mA/g, respectively, and the performance of PG, PB and PG-HT electrodes was compared at a current 111 mA/g. For the charge-discharge measurements, the upper cut-off voltage was set at 1.0 V and the lower cut-off voltage at 0 V with reference to Ag/AgCl (saturated KCl).

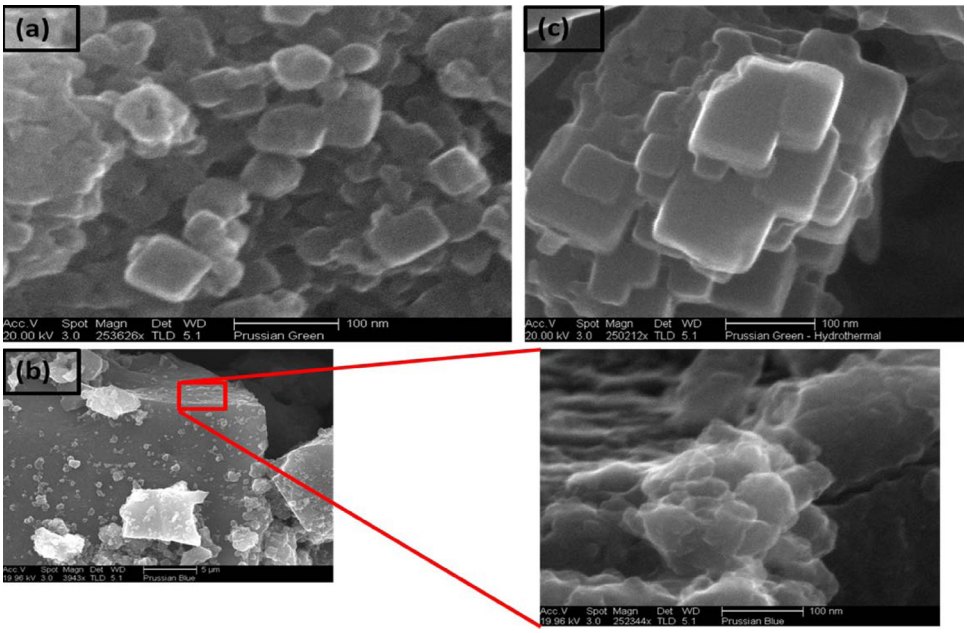

Fig. 2. SEM images of (a) Prussian green (PG). (b) Prussian Blue (PB) with magnified image of the surface of PB particles. Scale marker: 100 nm. (c). SEM image of hydrothermal Prussian Green (HT-PG).

3. Results and Discussion

Prussian Green (PG) and Prussian Blue (PB) allow for a dual step insertion and extraction of K^+ ions. PB is a partially reduced form of PG, with a very similar lattice structure to PG, and also possesses a theoretical gravimetric capacity of approximately 155.52 mAhr/g. In order to study the effect of further improved crystallinity of PG on the specific capacity, a fresh batch of Prussian Green (PG-HT) was synthesized using the hydrothermal technique as mentioned in the experimental section.

The SEM image of precipitated PG indicates highly crystalline polydispersed nanoparticles with sizes in the range of 50–75 nm, as shown in Fig. 2a. The PG nanoparticles also possess a porous texture, suitable for electrolyte diffusion through the active material. The SEM images of precipitated PB and PG-HT indicate large particles on the order of 2–10 microns, as shown in Figs. 2b and 2c, respectively. We attribute the differences in the synthesized particles sizes of PG and PB as being due to the differences in the reaction rates between potassium ferricyanide and potassium ferrocyanide with ferric nitrate. EDAX measurement indicated the presence of the following elements: Fe, C, N and K for PB and Fe, C, N and a very tiny fraction of K for PG. The atomic % of the above mentioned elements have been tabulated in Table 1.

The PXRD patterns of PG, PB and PG-HT are shown in Figs. 3a–3b. PG, PB and PG-HT were found to have face centered cubic (FCC) unit cells with almost identical lattice parameters of 10.2 Å. The XRD plot indicates that the PB powder was less crystalline than the PG. We attribute this difference in crystallinity to the different reaction rates and reaction pathways associated with the different precursors used for the synthesis of PB and PG. The XRD data in Fig. 3 indicates that PG-HT is more crystalline in nature than PG and possesses all the major peaks present in PG. However, in addition to the peaks related to PG, the following new peaks were identified in HT-PG: 12.7°, 15.7°, 19°, 20.4°, 21.3°. These additional peaks are highlighted by the symbol (*) in the magnified portion of the PXRD spectrum of PG-HT samples. We could not relate these peaks to any of the oxides and hydroxides of iron at this time and speculate that these additional peaks represent the presence of a small amount of unknown impurities from the by-products.

Table 1
EDAX data for PG and PB.

Element	Atomic % (PG)	Atomic %(PB)
C	39.30	26.57
N	56.47	35.83
K	0.08	4.84
Fe	4.15	32.12

The active material (PG, PB, PG-HT) electrodes were electrochemically characterized by cyclic voltammetry at a scan rate of 0.5 mV/sec, as presented in Figs. 4a–4d. The PG based electrodes exhibit a dual step insertion (0.20 V, 0.89 V) and extraction (0.239 V, 0.93 V) of K^+ ions into and from the PG lattice, respectively. The first pair of peak insertion (0.20 V) and extraction potentials (0.24 V) and the second pair of peak insertion (0.89 V) and extraction potentials (0.93 V) are also separated by 40 mV. The PB based electrodes also indicate a dual step insertion (0.177 V, 0.874 V) and extraction (0.234 V, 0.917 V) of K^+ ions into and from the PG lattice, respectively. The first pair of peak insertion (0.177 V) and extraction potentials (0.234 V) are separated by 57 mV and the second pair of peak insertion (0.874 V) and extraction potentials (0.917 V) are separated by 43 mV. The PG-HT based electrodes also indicate a dual step insertion (0.197 V, 0.893 V), but a three-step extraction (0.242 V, 0.81 V, 0.998 V) of K^+ ions into and out of the PG lattice, respectively. The first pair of peak insertion (0.197 V) and extraction potentials (0.242 V) are separated by 45 mV and the second pair of peak insertion (0.893 V) and extraction potentials (0.998 V) are separated by 105 mV.

The PG based electrodes demonstrated highly reversible insertion and extraction of K^+ ions as characterized by the CV in Fig. 4(a). The first step insertion of K^+ ions at 0.89 V leads to the formation of Prussian Blue (PB) and the second step insertion of K^+ ions at 0.2 V leads to the formation of Prussian White (PW) as shown below in Eqs. (1) and (2) below:

$$Fe^{III}Fe^{III}(CN)_6(PG) + K^+ + e^- \leftrightarrow KFe^{II}Fe^{III}(CN)_6\ (PB) \quad (1)$$

$$KFe^{II}Fe^{III}(CN)_6\ (PB) + K^+ + e^- \leftrightarrow Fe^{II}Fe^{II}(CN)_6\ (PW) \quad (2)$$

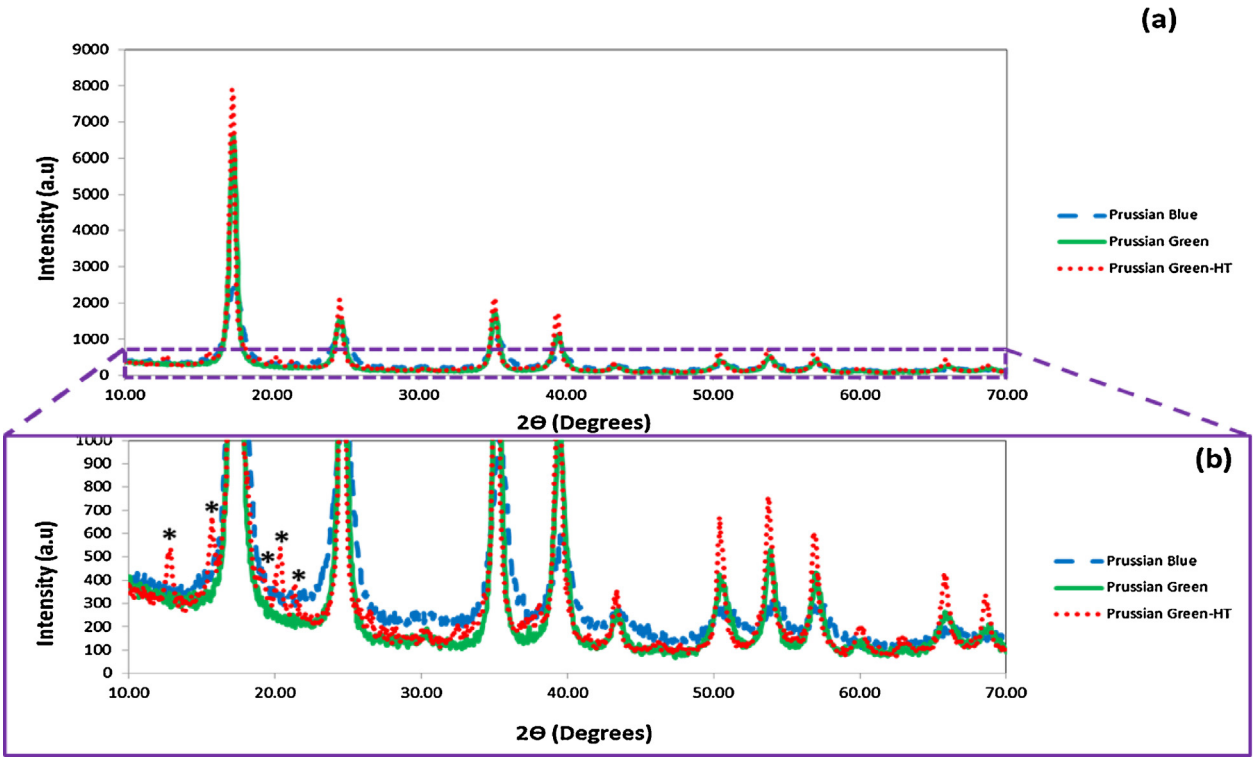

Fig. 3. (a). Powder XRD (PXRD) pattern of as synthesized PG, PB and PG-HT. (b). Magnified view of the PXRD pattern and reduced intensity. The peaks indicated by * represent unknown impurities.

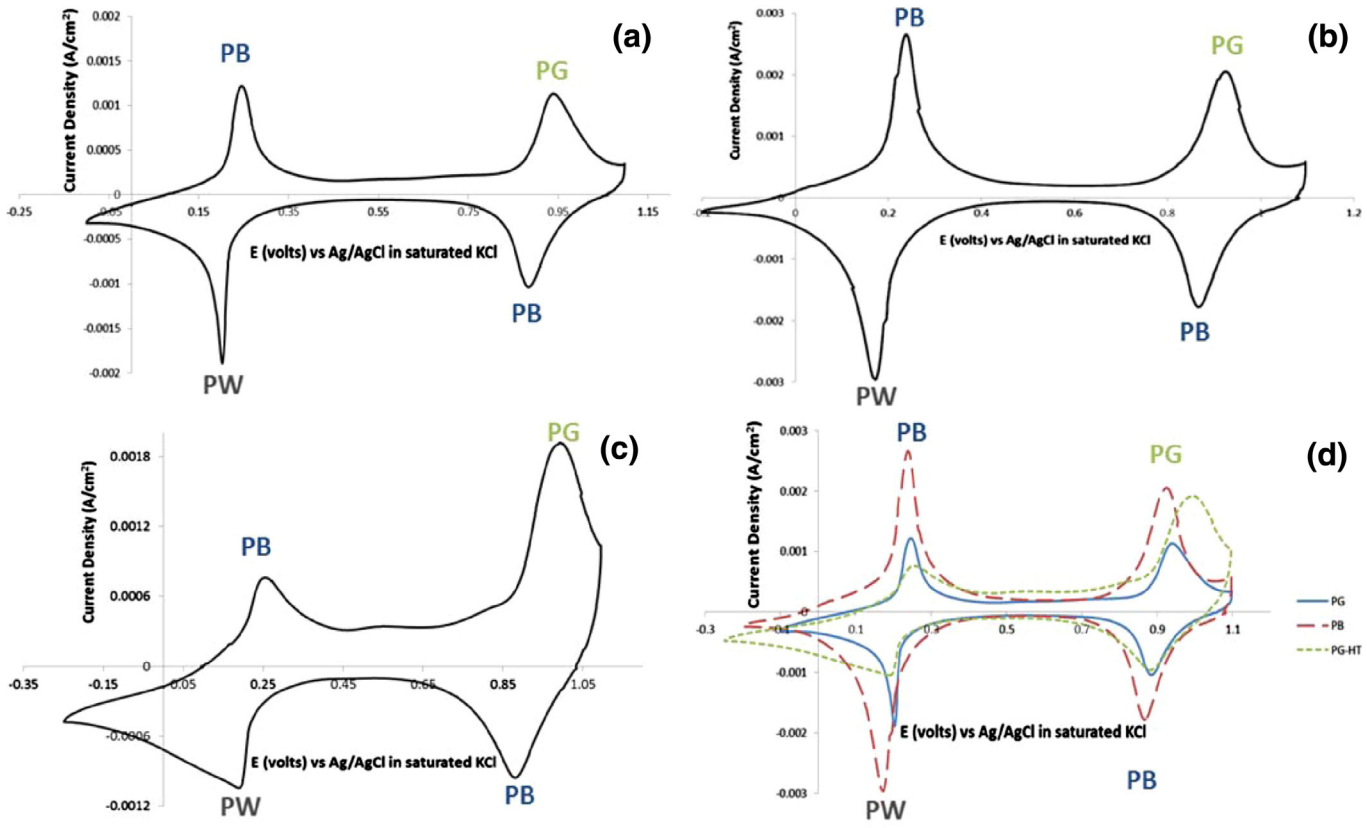

Fig. 4. Cyclic voltammograms (CV) of (a) PG electrode. (b) PB electrode. (c) PG-HT electrode. (d) Comparison of the CV curves of PG, PB and PG-HT electrodes. All the CV measurements were made in presence of KNO_3 electrolyte (pH = 2) using a scan rate of 0.5 mV/sec.

The PB based electrodes, like PG electrodes, demonstrated highly reversible dual step insertion and extraction of K^+ ions as characterized by CV (Fig.4b). The first step insertion of K^+ ions at 0.874 V leads to the formation of Prussian Blue (PB) and the second step insertion of K^+ ions at 0.177 V leads to the formation of Prussian White (PW). The cyclic voltammetry for PG-HT electrodes indicate a two-step insertion of K^+ ions, as indicated in Fig. 4(c). The first step insertion of K^+ ions at 0.874 V leads to the formation of Prussian Blue (PB) and the second step insertion of K^+ ions at 0.177 V leads to the formation of Prussian White (PW). However, the shape of the oxidation and reduction peaks indicates a quasi-reversible insertion and extraction of K+ ions.

The active material (PG, PB, PG-HT) electrodes were further subjected to galvanostatic cycling at a current density (J1) of 111 mA/g, as indicated by the galvanic cycling profiles in Figs. 5a–5c. Fig. 6a compares the specific capacity of PG, PB and PG-HT based electrodes at a current density of 111 mA/g. During the galvanic cycling measurement, insertion of K^+ ions was characterized as discharging, and the extraction of K^+ ions was characterized as charging. The PG electrodes were initially subjected to 20 cycles of charge-discharge measurements at a current density of 111 mA/g as shown by the charge-discharge profiles in Fig. 5(a), resulting in a gravimetric charge capacity of 121.4 mAhr/g and a discharge capacity of 123.08 mAhr/g, at the end of 20 cycles as shown in Fig. 6(a), compared to the theoretical gravimetric capacity of 155.52 mAhr/g. The PG electrodes also demonstrated very high coulombic efficiency of 98.7%, as indicated in Fig. 6(b), further illustrating the reversibility of K^+ ions in PG. The initial increase in the charge capacities and coulombic for all the materials (PG, PB and PG-HT) under consideration is due to the high open circuit potential of the electrodes, resulting in reduced amount of time required to reach the upper cut-off voltage. This reduction in time for the first cycle, results in a lower charge capacity. The charge-discharge profiles in Fig. 5(a), have two charge plateaus at 0.23 V and 0.91 V, indicative of a two-step extraction for K^+ ions from the PG lattice and two discharge plateaus at 0.217 V and 0.90 V, indicative of a two-step insertion of K^+ ions in to the PG lattice. The charge discharge plateaus resulting from the extraction and insertion of K^+ ions from the PG lattice are very flat, indicative of the minimal resistance encountered by the K^+ ions diffusing in and out of the lattice, resulting in a desirable feature of discharging at a constant power till the end of the battery capacity.

The PB electrodes were also further subjected to galvanic cycling measurements at a current density (J1) of 111 mA/g as shown in Fig. 5(b), resulting in a charge capacity of 54.2 mAhr/g and a discharge capacity of 53.8 mAhr/g at the end of 20 cycles as shown in Fig. 6(a), compared to a charge capacity of 121.4 mAhr/g

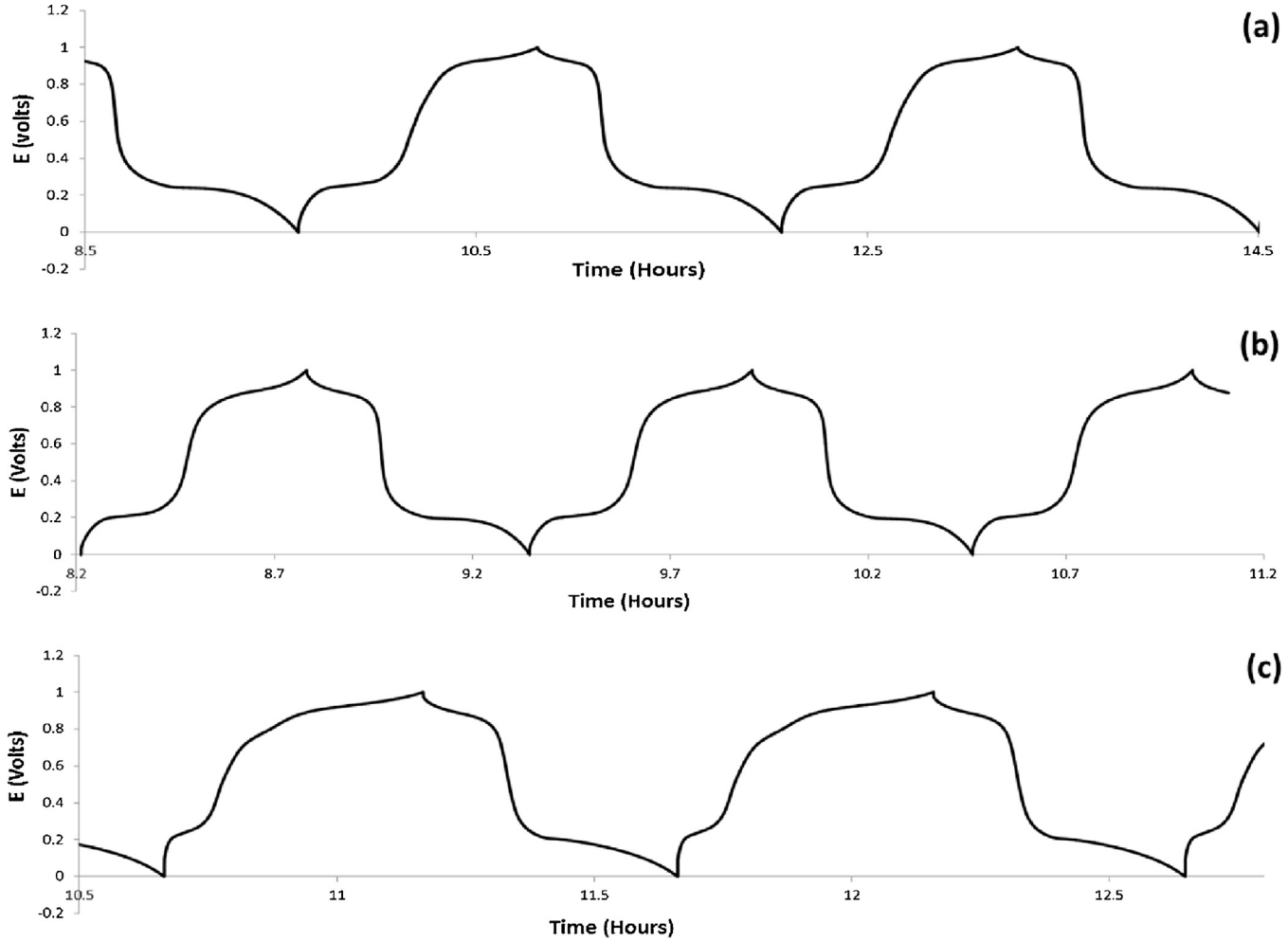

Fig. 5. Galvanostatic cycling (GC) of (a) PG electrode, (b) PB electrode, (c) PG-HT electrode. All the above GC measurements were made in presence of KNO_3 electrolyte (pH = 2) using a current density of 111 mA/g.

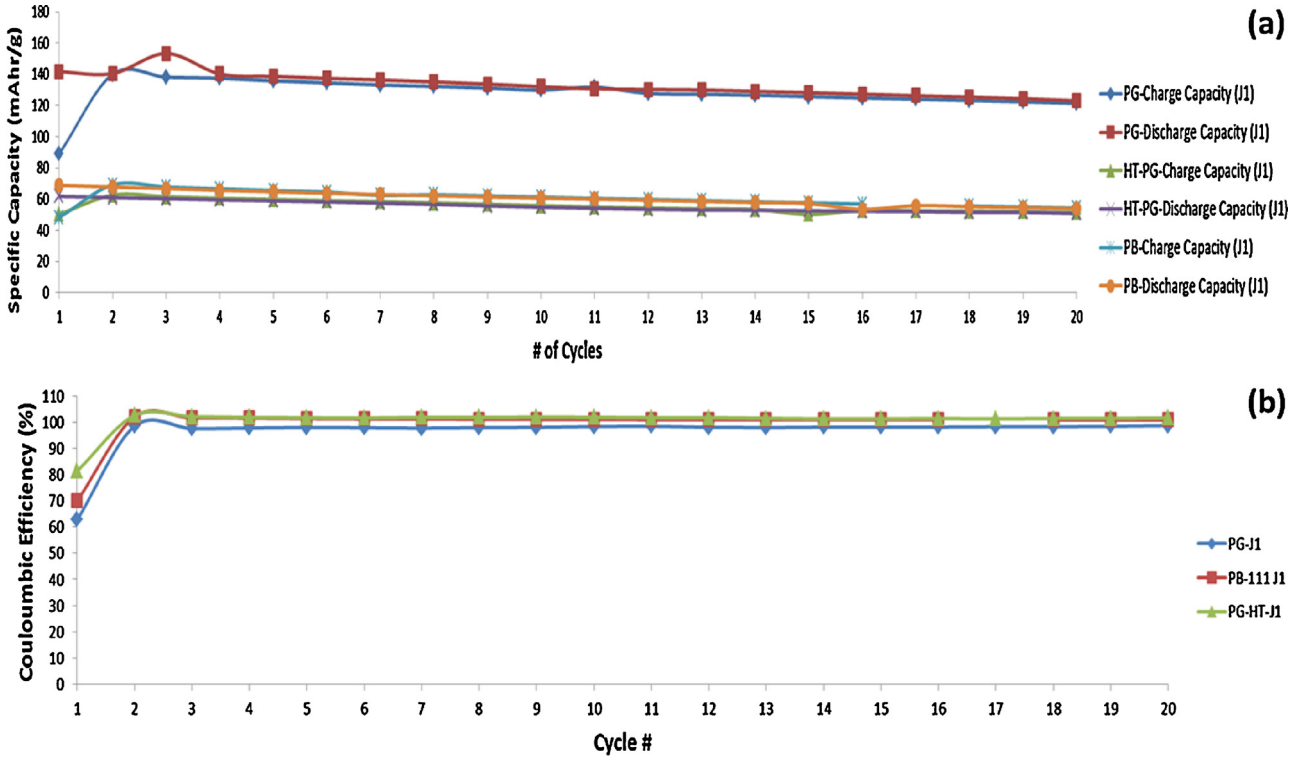

Fig. 6. (a). Comparison of specific capacity measurements of PG, PB, and PG-HT electrodes at a current density of 111 mA/g. (b). Comparison of coulombic efficiency (CE) of PG, PB and PG-HT electrodes at a current density of 111 mA/g.

and a discharge capacity of 123.08 mAhr/g for PG. The PB based electrodes exhibited excellent coulombic efficiencies of 100% throughout the 20 cycles as shown in Fig. 6(b). The charge-discharge profiles in Fig. 5(b) have two charge plateaus at 0.2 V and 0.8 V, indicative of a two-step extraction for K^+ ions from the PB lattice and two discharge plateaus at 0.19 V and 0.778 V, indicative of a two-step insertion of K^+ ions in to the PB lattice. We attribute the lower reversible capacities of PB based electrodes to the less crystalline nature of the synthesized PB (based on widths of x-ray peaks), along with the large diffusion lengths associated with large particle sizes on the order of several microns as shown in Fig. 2(b). These results demonstrate the importance of the sub-micron size of the crystalline particles of hexacyanoferrate based materials for performance as effective cathode materials for K^+ ion batteries.

The PG-HT electrodes were further subjected to galvanic cycling measurements at a current density (J1) of 111 mA/g as shown in Fig. 5(c). The charge capacity was measured to be 51.49 mAhr/g and the discharge capacity 50.70 mAhr/g at the end of 20 cycles as shown in Fig. 6(a), compared to a charge capacity of 121.4 mAhr/g and a discharge capacity of 123.1 mAhr/g for PG. The PG-HT electrodes exhibited excellent coulombic efficiencies of 100% throughout the 20 cycles as shown in Fig. 6(b). The charge-discharge profiles in Fig. 5(c), have three charge plateaus at 0.20 V, 0.747 V, 0.895 V, indicative of a three-step extraction for K^+ ions from the PG-HT lattice and two discharge plateaus at 0.19 V, 0.924 V, indicative of a two-step insertion of K^+ ions in to the PG-HT lattice. The presence of a third extraction potential and the absence of a corresponding third insertion potential could be indicative of the extraction of ions located at a different interstitial site associated with a different energy [11]. This behavior is also observed in the cyclic voltammetry measurements, which show the presence of three oxidation peaks at 0.242 V, 0.81 V, 0.998 V and two reduction peaks at 0.197 V, 0.893 V. The shape of the charge and discharge plateaus are relatively sloped compared to those of PG and PB, as shown in Fig. 5(a), 5(b), indicative of increased resistance encountered by the diffusing K^+ ions in the PG-HT lattice. We speculate that the lower capacities of PG-HT electrodes might be due to the large particles size (on the order of several microns), which presents large diffusion lengths to the K^+ ions, resulting in the under-utilization of the theoretical gravimetric capacity. Based on the above results, we believe that it is very important to have highly crystalline, defect-free hexacyanoferrate materials in the form of nanoparticles with short diffusion lengths for them to function as effective active materials for K^+ ion batteries.

With PG demonstrating the highest gravimetric capacity among the three materials, the PG electrodes were also subjected to galvanic cycling at three different current densities of 111 mA/g (J1), 277 mA/g (J2), and 388 mA/g (J3) to study the rate capability of the material as a cathode. Charge capacities of 121.4 mAhr/g, 94.98 mAhr/g, and 83.71 mAhr/g, respectively, were determined. Discharge capacities of 123.08 mAhr/g, 94.9 mAhr/g, and 83.6 mAhr/g were measured at the end of 20 cycles, accompanied by very high coulombic efficiencies of 98.7%, 100% and 100%, as shown in Figs. 7a and 7b. The retention of a reversible capacity of 83.71 mAhr/g at a current density of 388 mA/g, illustrates the ability of PG to deliver high capacities at high current densities, which is a result of fast diffusion of K^+ ions within the PG lattice. The size of hydrated K^+ ions is about 1.25 Å, which is smaller than the 1.6 Å size of the opening of the interstitial tunnel in PG based on the hard sphere model leading to easy insertion and extraction of fully hydrated K^+ ions from the lattice [12]. The presence of a complete hydration sheath around the intercalation/de-intercalating K^+ ions may minimize electrostatic interactions between the PG host lattice and the K^+ ions, resulting in fast diffusion and hence high rate capability of PG electrodes with hydrated K^+ ions. In order

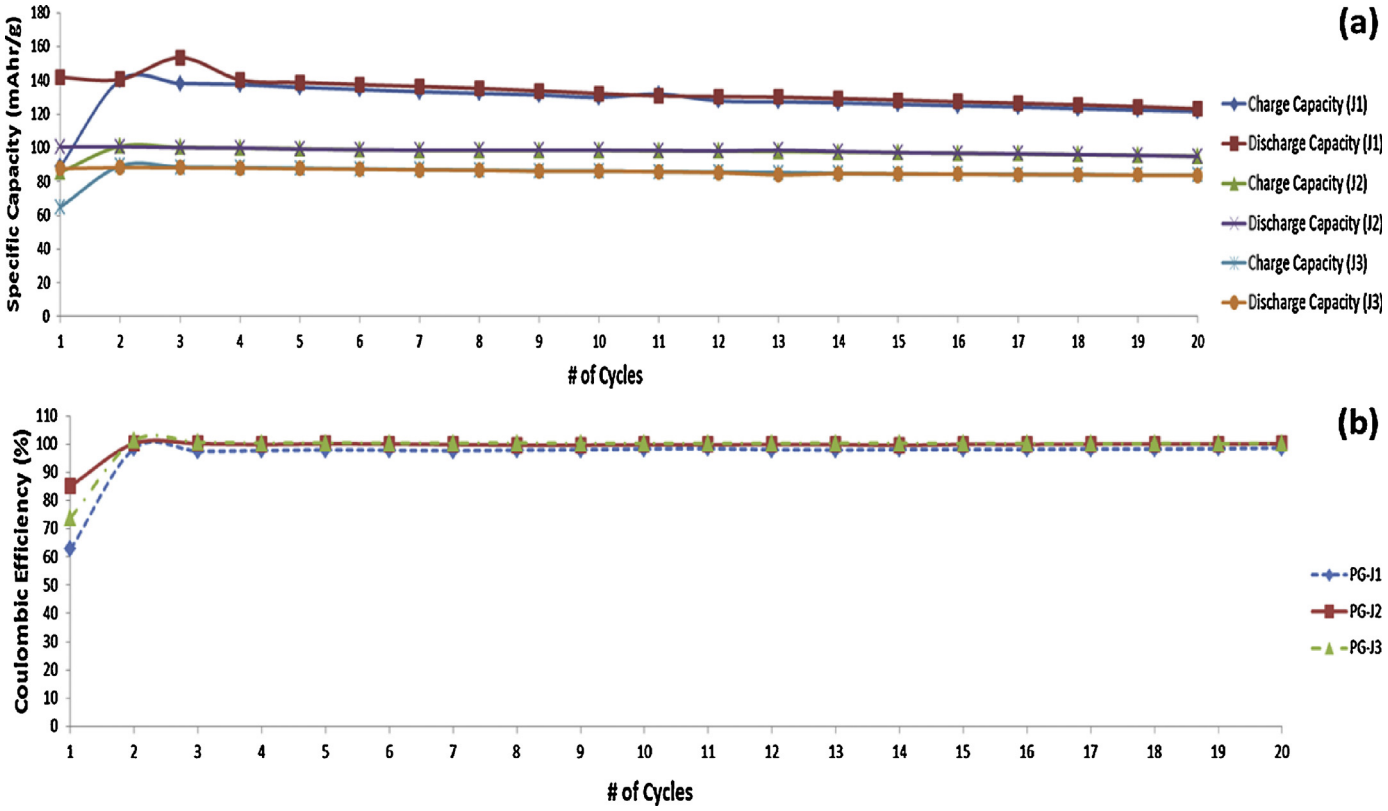

Fig. 7. (a). Rate capability measurements of PG electrodes at the following current densities: 111 mA/g, 277 mA/g, 388 mA/g. (b). Comparison of coulombic efficiency (CE) of PG electrodes at the following current densities: 111 mA/g, 277 mA/g, 388 mA/g.

to study capacity retention over large number of charge-discharge cycles, electrodes of PG and PB electrodes were subjected to charge-discharge cycling at a very high current density (J4) of 500 mA/g for 1100 cycles. The PG electrodes demonstrated an initial reversible capacity of 63.8 mAhr/g and a final reversible capacity of 30.27 mAhr/g, resulting in a capacity retention of 44.7% at the end of 1100 cycles. In comparison, PB electrodes demonstrated an initial reversible capacity of 49.16 mAhr/g and a final reversible capacity of 11.25 mAhr/g, as shown in Fig. 8(a), resulting in a capacity retention of 22.8% at the end of 1100 cycles. Both, PG and PB electrodes demonstrated a coulombic efficiency of 100%, as shown in Fig. 8(b).

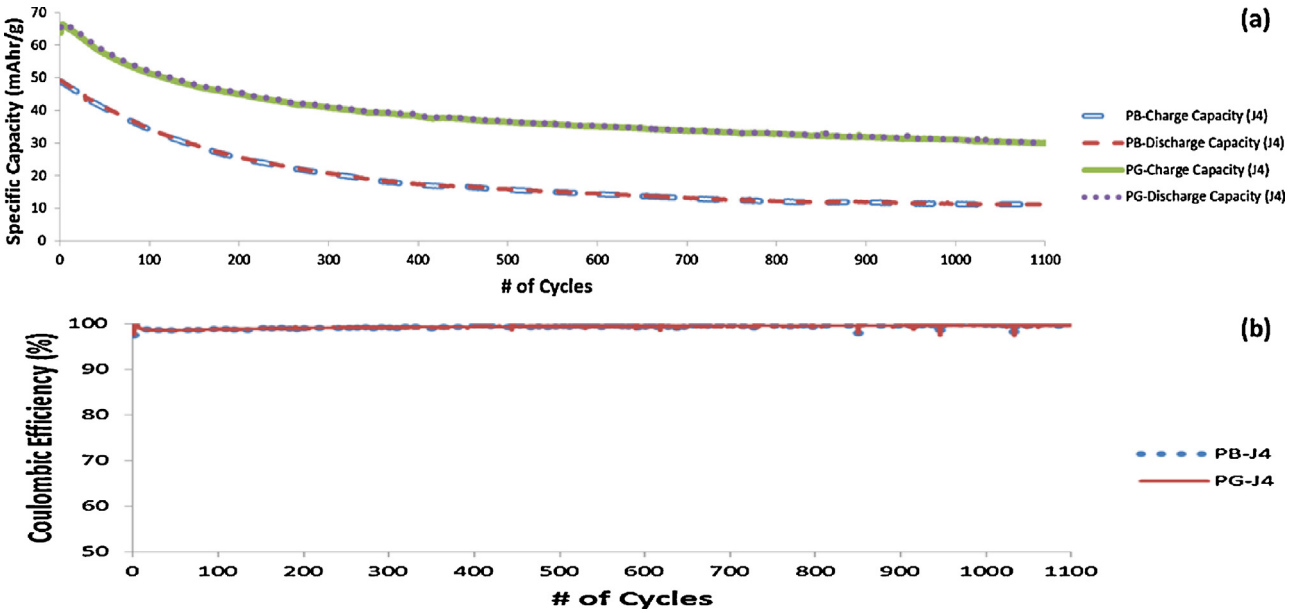

Fig. 8. (a). Rate capability measurements of PG and PB electrodes at a current density of 500 mA/g. (b). Comparison of coulombic efficiency (CE) of PG and PB electrodes at a current density of 500 mA/g. The coulombic efficiency of PG and PB electrodes are 100% and overlap with each other.

4. Conclusion

PB and PG were synthesized using different precursors, namely, potassium ferrocyanide and potassium ferricyanide, respectively. These precursors have different rates of reaction, resulting in different sizes of PB and PG particles. The particles of PG were much smaller in size compared to PB (50–75 nm compared to 2–10 um), which translates to much smaller diffusion lengths, thereby leading to enhanced capacity utilization of the host material in the case of PG electrodes as compared to PB electrodes (121.4 mAh/g compared to 53.8 mAh/g). The capacity increase for small particle size PG cathode materials in K+ ion batteries compares favorably with many of today's Li+ ion batteries, and may lead to a new generation of cheaper, safer battery materials for large scale energy storage.

Acknowledgements

We would like to thank Arkema for providing us with HSV900 PVDF binder. We would also like thank Sheng Kuei Chiu from Dr. Goforth's lab for helping us with the PXRD measurements.

References

[1] H.H. Kamerbeek, A.G. Rauws, M. ten Ham, A.N.P. van Heijst, Prussian blue in therapy of thallotoxicosis, Acta Med. Scand. 189 (1971) 321–324.
[2] F. Ricci, G. Palleschi, Sensor and biosensor preparation, optimisation and applications of Prussian blue modified electrodes, Biosens. Bioelectron. 21 (2005) 389–407.
[3] D. Moscone, D. D'ottavi, D. Compagnone, G. Palleschi, A. Amine, Construction and analytical characterization of Prussian blue-based carbon paste electrodes and their assembly as oxidase enzyme sensors, Anal. Chem. 73 (2001) 2529–2535.
[4] A. Eftekhari, Potassium secondary cell based on Prussian blue cathode, J. Power Sources 126 (2004) 221–228.
[5] Y. Lu, L. Wang, J. Cheng, J.B. Goodenough, Prussian blue: a new framework of electrode materials for sodium batteries, Chem. Commun. 48 (2012) 6544–6546.
[6] M. Jayalakshmi, F. Scholz, Charge-discharge characteristics of a solid-state Prussian blue secondary cell, J. Power Sources 87 (2000) 212–217.
[7] M. Pasta, C.D. Wessells, R.A. Huggins, Y. Cui, A high-rate and long cycle life aqueous electrolyte battery for grid-scale energy storage, Nat. Commun. 3 (2012) 1149.
[8] N. Imanishi, T. Morikawa, J. Kondo, Y. Takeda, O. Yamamoto, N. Kinugasa, T. Yamagishi, Lithium intercalation behavior into iron cyanide complex as positive electrode of lithium secondary battery, J. Power Sources 79 (1999) 215–219.
[9] M. Jayalakshmi, F. Scholz, Performance characteristics of zinc hexacyanoferrate/Prussian blue and copper hexacyanoferrate/Prussian blue solid state secondary cells, J. Power Sources 91 (2000) 217–223.
[10] K. Kuwabara, J. Nunome, K. Sugiyama, Rechargeability of solid-state copper cells utilizing cathodes of Prussian blue and Berlin green, Solid State Ionics 48 (1991) 303–308.
[11] H. Lee, Y.I. Kim, J.K. Park, J.W. Choi, Sodium zinc hexacyanoferrate with a well-defined open framework as a positive electrode for sodium ion batteries, Chem. Commun. 48 (2012) 8416–8418.
[12] C.D. Wessells, S.V. Peddada, M.T. McDowell, R.A. Huggins, Y. Cui, The effect of insertion species on nanostructured open framework hexacyanoferrate battery electrodes, J. Electrochem. Soc. 159 (2011) A98–A103.
[13] H.D.B. Jenkins, D.F.C. Morris, Crystal radius and enthalpy of hydration of the cyanide ion. Lattice energies of alkali metal cyanides, enthalpy of formation of CN-(g) and the electron affinity of the cyanide radical, Molecular Physics 33 (3) (1977) 663–669.
[14] H.J. Buser, D. Schwarzenbach, W. Petter, A. Ludi, The crystal structure of Prussian blue: Fe4 [Fe (CN) 6] 3. xH2O, Inorganic Chemistry 16 (1977) 2704–2710.